Available online at website: https://journal.bcrec.id/index.php/bcrec

Bulletin of Chemical Reaction Engineering & Catalysis, 21 (1) 2026, 80-95

Original Research Article

Green Synthesis of ZnO Nanoparticles using Aloe Vera Extract and Xanthan Gum as Modifier for Photocatalytic Degradation of Anionic and Cationic Dye in Aqueous Solution

Imelda Fajriati*, Priyagung Dhemi Widiakongko, Didik Krisdiyanto, Heti Hermawati

Department of Chemistry, Universitas Islam Negeri (UIN) Sunan Kalijaga, Yogyakarta 55282, Indonesia.

Received: 24th September 2025; Revised: 2nd December 2025; Accepted: 3rd December 2025
Available online: 20th December 2025; Published regularly: April 2026

Abstract

The green synthesis of Zinc Oxide (ZnO) nanoparticles is a simpler, low-energy method that avoids toxic chemicals, making the process more cost-effective and environmentally friendly. The green synthesis was performed using aloe vera extract (55% - Aloin), rich in electrons from its hydroxyl groups, as a reducing agent, and natural polysaccharides from xanthan gum to disperse particles and prevent agglomeration. The green synthesis product was characterized using scanning electron microscopy, Fourier Transform spectroscopy, X-ray diffraction, transmission electron microscopy, and Diffuse Reflectance UV spectroscopy. The green-synthesized ZnO nanoparticles, both with xanthan gum (ZnO-AL/XG) and without xanthan gum (ZnO-AL), adopted a hexagonal wurtzite crystal structure. The addition of xanthan gum significantly reduced the crystallite size and enhanced the surface homogeneity of the photocatalyst. Over 50% removal of both anionic and cationic dyes was achieved by ZnO-AL/XG for up to 3 uses, and by ZnO-AL for up to 2 uses, respectively. These findings highlight the potential of the aloe vera–xanthan gum-based green synthesis as a sustainable and efficient strategy for producing ZnO nanomaterials applicable in dye wastewater treatment.

Keywords: Green synthesis; ZnO nanoparticles; Aloe vera extract; Photocatalytic degradation

How to Cite: Fajriati, I., Widiakongko, P. D., Krisdiyanto, D., Hermawati, H. (2026). Green Synthesis of ZnO Nanoparticles using Aloe Vera Extract and Xanthan Gum as Modifier for Photocatalytic Degradation of Anionic and Cationic Dye in Aqueous Solution. *Bulletin of Chemical Reaction Engineering & Catalysis*, 21 (1), 80-95. (doi: 10.9767/bcrec.20495)

Permalink/DOI: https://doi.org/10.9767/bcrec.20495

1. Introduction

One effective method to reduce aquatic waste is an advanced oxidation process (AOP) based on the Fenton reaction. AOP is an advanced oxidation process using photocatalysts, usually iron oxide, and hydrogen peroxide (H_2O_2) producing hydroxyl radicals ($\bullet OH$) that are very reactive, breaking down toxic pollutants such as organic dyes, pesticides, phenol compounds, and heavy metals. These poisonous pollutants adversely affect human health, harm aquatic biota, and degrade water quality. AOP reaction conditions should focus on the pH range and post-reaction regeneration techniques, as the photocatalyst readily precipitates in alkaline pH [1]. The advantages of the AOP method include environmental friendliness, rapid reaction times, and the simultaneous breakdown of pollutants into simple, non-toxic minerals and the detoxification of heavy metals [2].

Zinc oxide (ZnO), a semiconducting metal oxide, is a photocatalyst with a band gap energy of 3.37 eV and an exciton binding energy of 60 meV that is effective in treating wastewater through advanced oxidation processes (AOPs). ZnO is renowned for its outstanding electrical, mechanical, and optical properties. The excellent photocatalytic properties of ZnO make it a widely utilized material for the degradation of contaminants in wastewater. To enhance its photocatalytic activity, ZnO is commonly

* Corresponding Author.
Email: imelda.fajriati@uin-suka.ac.id (I. Fajriati)

prepared in the form of nanoparticles. However, traditional wet chemical synthesis techniques are gradually being replaced due to the production of hazardous byproducts that can threaten the environment and human health. Consequently, increasing attention has been directed to green synthesis approaches, which offer greater environmental sustainability, cost efficiency, biocompatibility, and reduced health risks [3]. These environmentally friendly methods generally involve simpler protocols, lower energy requirements, and minimal waste generation while adhering to sustainable practices [4].

Green synthesis of ZnO nanoparticles can be achieved using various biological materials, including plant extracts (from leaves, fruits, flowers, stems, or roots), microorganisms (such as bacteria, fungi, and algae), and other forms of biomass. These sources are rich in phytochemicals that function as both reducing agents (usually antioxidants) and stabilizing ligands during nanoparticle formation [5]. Phytochemical constituents play a crucial role in transforming zinc precursors into nanoparticles by facilitating the reduction and stabilization of metal ions. Key bioactive compounds participating in this mechanism include terpenoids, flavonoids, phenolics, aldehydes, and alkaloids, as well as individual molecules such as ursolic acid, oleanolic acid, ß-sitosterol, rutin, leucocyanidin, anthocyanins, proanthocyanidins, and glycoside forms of kaempferol and quercetin, which collectively drive the reduction process [6,7]

The efficiency of phytochemical-assisted reduction processes is influenced by the concentration and specific chemical composition of plant extracts, which in turn regulate the size, morphology, and crystal structure of the synthesized ZnO nanoparticles [8]. The use of plant extracts also introduces inconsistencies in plant maturity and fluctuations in phytochemical content, posing significant obstacles to reproducibility. This challenge in determining the concentration of bioactive compounds in plant extractsts in particle agglomeration [9] and poor crystallinity [10,11].

One of the plant extracts widely studied is Aloe vera (family Liliaceae), which is used in food, cosmetics, and photocatalysis [12]. Aloe barbadensis miller leaf extract has been successful as a reducing agent in the synthesis of ZnO nanoparticles. However, as with the use of plant extracts in green synthesis, the use of aloe vera must consider several variables, such as volume, reaction time, precursor concentration, and temperature [13]. One of the difficulties in green synthesis is the formation of agglomerates and aggregates of metal ions [14], which tend to form bulk and make it difficult in determine the optimum reaction concentration.

Aloe vera leaf extract is composed of over 75 biologically active constituents, including phenolic acids, polysaccharides, saponins, flavonoids, alkaloids, terpenoids, and anthraquinone derivatives such as Aloin and aloe-emodin [15]. As a natural anthraquinone, Aloin is mainly concentrated in the latex of some aloe species [16,17]. Aloin is particularly well known for its high hydroxyl content, which enables it to act effectively as a reducing and stabilizing agent in nanoparticle synthesis [18]. The reduction and stabilization mechanism involves the encapsulation of metal ions with organic compounds through a three-phase process [16]: (1). Activation Phase: In this stage, the metal ions undergo reduction, accompanied by nucleation of the reduced ions; (2). Growth Phase: Phytochemical matrices stabilize the growing nanoparticles; (3). Termination Phase: Growth ceases, leading to nanoparticle formation.

The green synthesis of ZnO nanoparticles investigated the use of aloe vera extract in the form of Aloin as a reducing and stabilizing agent, and xanthan gum to suppress the agglomeration and aggregation of metal ions. Xanthan gum enhances dispersion stability through its D-gluconate chains, which regulate nanoparticle growth and support the crystallization of ZnO nanostructures [19]. Nanoparticle formation occurs within the polysaccharide matrix, which acts as an intrinsic reducing and capping medium due to its richness in functional groups. This strategy avoids the use of surfactants or additional capping agents that may introduce residual contaminants [20].

Polysaccharide chains envelop the formed nanoparticles, effectively inhibiting aggregation while controlling their size and morphological characteristics. The involvement of extracellular polysaccharides has been shown to enhance crystallinity and facilitate uniform dispersion of nanoparticles, as illustrated by the proposed mechanism in Figure 1.

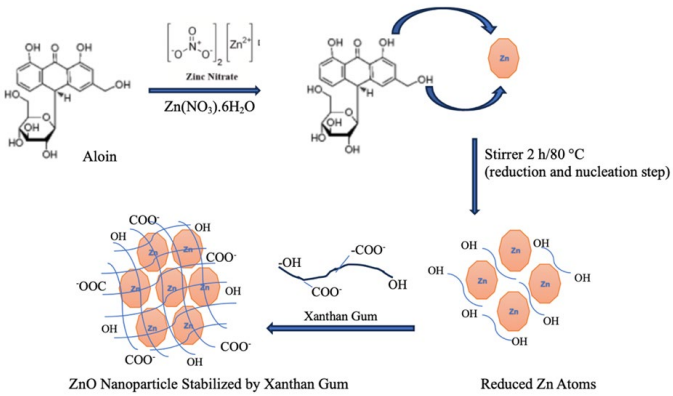

Figure 1. Proposed mechanisms for the green synthesis of ZnO nanoparticles using aloe vera extract (55% ~ Aloin) and Xanthan Gum as a modifier.

The chemical processes underlying green synthesis are inherently complex, often involving multiple reaction pathways that complicate the identification and quantification of the specific molecules responsible. Nevertheless, it is generally recognized that polysaccharide biomolecules act as electron donors to reduce metal ions, while additional components in the biological matrix serve to coat the nanoparticle surface, restrict particle growth, prevent aggregation, and modify the surface characteristics of the resulting nanoparticles [21].

The photocatalytic activity of the synthesized ZnO nanoparticles was tested for the degradation of Remazol Yellow, an anionic dye, and Rhodamine B, a cationic dye (Figure 2). Those dyes were widely used in the textile industries and potentially hazardous to the water environment. Rhodamine B (RB) is one of the positively charged basic dyes (usually amine salts or ionized imines) because RB ionized Cl^-, and on the other hand, Remazol Yellow (RY) is an acidic dye with a negative charge (usually an organic sulfonate group, RSO_2O^-) because RY ionizes Na^+ in solution. The molecular structures of Rhodamine B (RB) and Remazol Yellow (RY) are shown in Figure 2. The results of this study provide a method for synthesizing energy-efficient and environmentally friendly photocatalysts. The successful green synthesis of ZnO nanoparticles using aloe vera extract and xanthan gum offers novelty as an alternative for preparing ZnO as a photocatalyst for the photodegradation of dyes.

2. Materials and Methods

2.1 Materials

In this research, the following materials were utilized, Aloin powder (~50% content extracted from Curacao aloe ($C_{21}H_{22}O_9$; Sigma-Aldrich), zinc nitrate hexahydrate ($Zn(NO_3)_2 \cdot 6H_2O$; Sigma-Aldrich), xanthan gum derived from Xanthomonas campestris (Sigma-Aldrich), absolute ethanol 99.8% (CH_3CH_2OH, Merck), pyridine (C_5H_5N; Merck), glacial acetic acid (CH_3COOH; Merck), Remazol Yellow ($C_{18}H_{13}N_2S_4O_{12}Na_3$; Merck), Rhodamine B ($C_{28}H_{31}ClN_2O_3$; Merck), ammonium hydroxide 25% (NH_4OH; Merck), ammonium chloride (NH_4Cl; Merck), anhydrous sodium acetate (CH_3COONa; Merck), and distilled water.

2.2 Preparation of Aloe Vera Extract

Aloe vera extract was prepared by dissolving 1 gram of Aloin powder in 10 mL of pyridine, then diluting the mixture to 250 mL in a measuring flask. An Aloin concentration of 40 ppm was stirred at 80 °C for 2 hours, and the resulting solution was stored for later use.

2.3 Preparation of Xanthan Gum Gel

Xanthan gum gel was prepared by dissolving 0.4 g of xanthan gum powder in 100 mL of distilled water (0.004 g/mL) and stirring continuously at room temperature for 24 hours until a homogeneous gel formed.

2.4 Green Synthesis of ZnO Nanoparticles

ZnO-Al; 50 mL of $Zn(NO_3)_2 \cdot 6H_2O$ 0.25 M was dissolved in absolute ethanol and stirred at 60 °C for 30 minutes. Aloe vera extract (0.5 M) was then added to reach a final volume of 250 mL. The mixture was stirred for 2 hours at 80 °C and allowed to stand overnight. The resulting pale white precipitate was washed, centrifuged at 4000 rpm, and then calcined at 700 °C for 3 hours.

ZnO-AL/XG; Following the same procedure as above, after 2 hours of stirring at 80 °C, 1 mL of 0.2% (b/v) xanthan gum gel and 10 mL of NaOH 0.01 M were added to the $Zn(NO_3)_2$ Aloe vera mixture. The solution was stirred again for 2 hours at 80 °C and calcined at 700 °C for 3 hours to obtain ZnO nanoparticles.

2.5 Characterization of ZnO nanoparticle as Photocatalyst

Characterisation of ZnO nanoparticles was conducted to evaluate their photocatalytic properties. The structure, phase composition, and average crystallite size of the ZnO nanoparticles were determined using powder and plate X-ray diffraction (XRD). Diffraction patterns were obtained with a Shimadzu X-ray Diffractometer

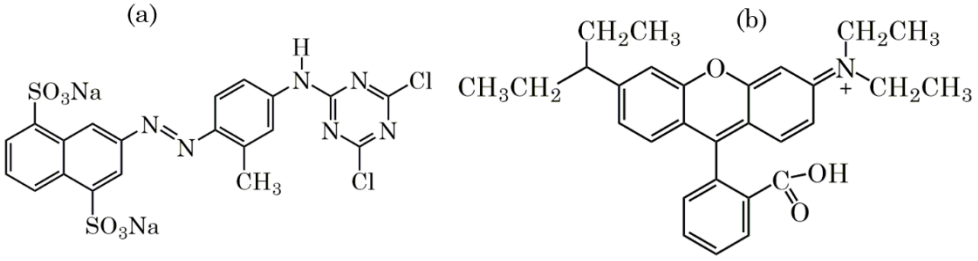

Figure 2. The molecular structure of (a) Remazol Yellow and (b) Rhodamine B.

6000, equipped with a Cu-Kα radiation source (λ = 1.5460 Å) operated at 40 kV and 30 mA, with a scanning rate of 1° min^{-1} over the 2θ range of 20–80°. The functional groups were analyzed by Fourier Transform Infrared Spectroscopy (FTIR, Shimadzu) using KBr pellets in the spectral range of 400–4000 cm^{-1}. Surface morphology was examined using a Scanning Electron Microscope (SEM, JEOL JSM–6360). The microstructure and information on size, shape, and crystal phase were studied using a Transmission Electron Microscope (TEM, JEOL JEM-1400). The optical properties were assessed by diffuse reflectance UV–Vis spectroscopy (Shimadzu UV-1700 Pharmaspec). The decolorization of RY and RB was monitored Spectrophotometric UV-1280 Shimadzu.

A magnetic stirrer hotplate (Cimarec Barnstead Thermolyne) was employed for solution preparation, while centrifugation was performed using a Boeco C-28 Centrifuge (Model BOE 1205-13, Boeckel & Co., Hamburg, Germany). The drying process was carried out in a laboratory oven (Thermoline Electric, Heraeus). Photocatalytic degradation of RY and RB was conducted in a closed photoreactor equipped with a 40 W UV lamp operating in the wavelength range of 290–390 nm, together with a magnetic stirrer to ensure homogeneous mixing.

2.6 Photocatalytic degradation of Cationic and Anionic Dye in Aqueous Solution

The experiment of photocatalytic degradation of Cationic and Anionic Dye by ZnO Nanoparticle was carried out by dispersing 0.1 g of each ZnO-AL and ZnO-AL/XG with 30 mL of RY (25 and 50 mg/L) and RB (10 and 20 mg/mL) in an Erlenmeyer flask. The solution mixture was irradiated with a 40 W UV lamp (290–390 nm) for 60, 120, 180, 240, 300, and 360 minutes. The solution pH was adjusted to 2, 4, 6, 8, 10, and 12 using sodium acetate and ammonium chloride buffers.

Photocatalytic degradation studies were conducted in a flask on a magnetic stirrer, with stirring time adjusted to account for the presence of vertically incident UV light. A 10 mL sample was taken every 60 min of interval time using a syringe. The solution was centrifuged, and the supernatant was analyzed by UV spectrophotometry at 425 nm (RY) and 542 nm (RB). The degradation efficiency of dyes was calculated using the following equation:

$$\%\ Degradation\ dyes = \frac{(C_i - C_t)}{C_i} \times 100\% \quad (1)$$

$$\%\ Degradation\ dyes = \frac{(A_i - A_t)}{A_i} \times 100\% \quad (2)$$

where, C_i, A_i are initial concentrations (mg/L) and initial absorption of Dyes and C_t, A_t, are represents the dyes concentration (mg/L) and absorption after a certain irradiation time (t).

3. Results and Discussion

3.1 Characterization of ZnO nanoparticles as a Photocatalyst

Characterization of ZnO nanoparticles was carried out using FTIR, XRD, DRUV, SEM and TEM analyses. The ZnO nanoparticles was also tested for photocatalytic degradation of Cationic and Anionic Dye using spectrophotometric methods.

3.1.1 Fourier Transform Infrared Spectroscopy

Functional groups of ZnO-AL and ZnO-AL/XG were characterized by Fourier Transform Infra-Red (FTIR) Spectroscopy. Figure 3

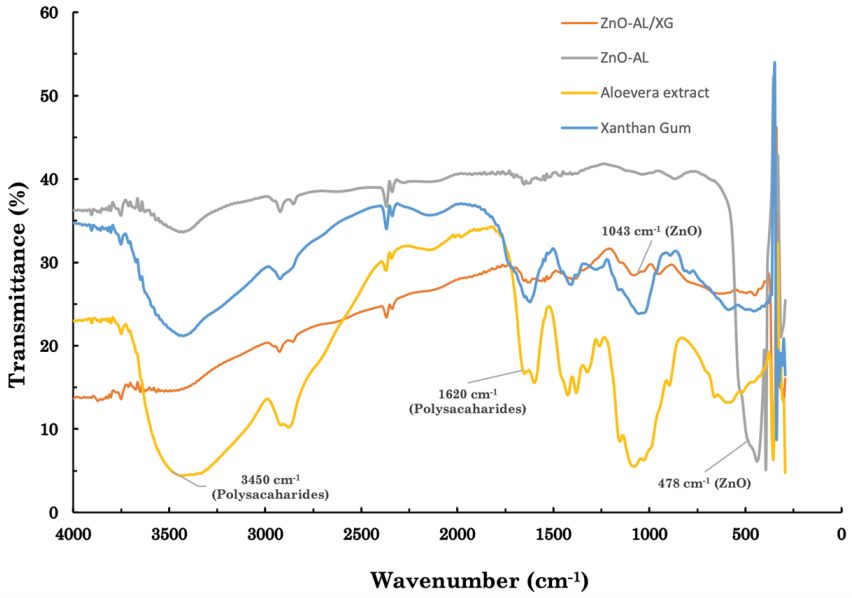

Figure 3. FTIR spectra (4000 – 400 cm−1) for ZnO-AL/XG, Aloe vera extract, xanthan gum powder, and ZnO-AL.

compares the FTIR spectra of xanthan gum powder, ZnO-AL, ZnO-AL/XG, and Aloe vera extract.

The FTIR spectra confirmed the characteristic Zn–O bond vibrations at 478.35 cm^{-1}, typical of metal oxide frameworks. An absorption band observed at 1043 cm^{-1} was assigned to the asymmetric stretching of the glycosidic C–O–C bridge. Low-intensity peaks at 992 cm^{-1} and 852 cm^{-1} were associated with ß-glycosidic linkages between cellulose-derived sugar units of aloe vera involved in the synthesis of ZnO nanoparticles. In contrast, the peak at 1635 cm^{-1}, corresponding to amine and phenolic groups, and the band at 1620 cm^{-1}, attributed to C=C and C=O stretching in aromatic and flavonoid structures, disappeared in the spectra of the final ZnO materials. These spectral modifications provide strong evidence for the involvement of aloe vera bioactive compounds in nanoparticle formation [21].

The absorption peak at 2916 cm^{-1}, corresponding to C–H stretching in long-chain hydrocarbons, together with the strong O–H band at 3450 cm^{-1}, typically associated with polysaccharides in xanthan gum and aloe vera, disappeared in the spectra of ZnO-AL/XG and ZnO-AL. This disappearance further supports the involvement of these functional groups in the nanoparticle formation process. The broad absorption at 3450 cm^{-1}, associated with –OH groups in aloe vera and xanthan gum [22], was diminished in ZnO-AL/XG, suggesting coordination with Zn^{2+} ions. The reduction and stabilization of Zn^{2+} to ZnO may have been achieved by the donation of electrons (lone pairs) from oxygen inside an XG–O–Zn type lattice, as shown by a shift in the vibrational frequency of the carboxylic acid [23].

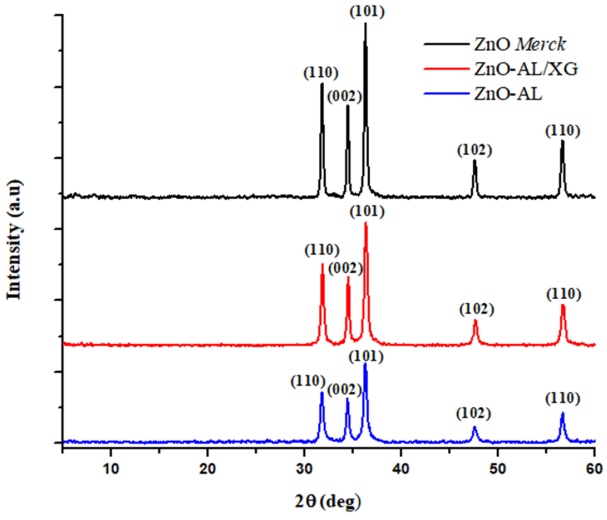

Figure 4. XRD Patterns of ZnO-AL/XG, ZnO-AL, and ZnO Merck.

Although it is difficult to understand how plant extracts are involved in the biosynthesis of nanoparticles, FTIR analysis results indicate that the redox reactions occurring during the glycolysis process may be the mechanism used by zinc ions to interact with plant phytochemicals. After the production of adenosine triphosphate (ATP), there are many H^+ ions that function as reductants. The process is supported by the coenzyme nicotinamide adenine dinucleotide (NAD), which is found in all living cells. NAD is a strong oxidizing agent that accepts electrons from other molecules, which can donate them during the reduction process. As a result, this redox process continues to repeat in a cycle, reducing zinc ions to zero zinc. As in the following reaction:

$$Zn(NO_3)_2 \rightarrow Zn^{2+} + NO_3^- \quad (3)$$

$$2NAD^+ + 2e^- \rightarrow 2NAD \quad (4)$$

$$2NAD^+ + 2H \rightarrow 2NADH + 2e^- \quad (5)$$

$$Zn^{2+} + 2e^- \rightarrow Zn^0 \quad (6)$$

The observed transformations suggest that phytochemicals such as NAD^+ and related reductants facilitate electron transfer during redox reactions, ultimately reducing Zn^{2+} ions to Zn^0. This process may proceed via a glycolytic mechanism, in which NADH serves as an effective electron donor.

3.1.2 X-Ray Diffraction Spectroscopy

X-ray diffraction (XRD) analysis was performed to verify the crystalline phases and polymorphs of ZnO. The diffraction pattern of ZnO-AL/XG, presented in Figure 4, exhibited distinct peaks at 2θ values of 31.8°, 34.4°, 36.2°, 47.5°, and 56.6°, which are characteristic of the hexagonal wurtzite crystal structure. These reflections correspond well with the Joint Committee on Powder Diffraction Standards (JCPDS) card No. 36-1452 and can be indexed to the (100) and (101) crystal planes [24].

A careful examination of Fig. 4 reveals that the incorporation of xanthan gum enhances the crystalline phase content of ZnO-AL/XG, as evidenced by the higher relative peak intensity compared to ZnO-AL. This observation is consistent with previous reports. Furthermore, the sharpness of the XRD peaks reflects the particle size of the ZnO nanoparticles, with narrower peaks indicating smaller crystallite dimensions. The average crystallite size of ZnO nanoparticles was estimated from the XRD line broadening using the Debye–Scherrer equation:

$$L = \frac{K\lambda}{\beta \cos\theta} \quad (7)$$

The average crystallite size (L) of ZnO nanoparticles was calculated using the Debye–

Scherrer equation, where L represents the crystallite size (nm), K is Scherrer's constant (0.94), λ is the X-Ray wavelength (Cu-Kα = 1.54056 Å), β denotes the full width at half maximum (FWHM) of the diffraction peak, and θ is the Bragg diffraction angle at the peak centroid. The estimated average crystallite sizes of ZnO–AL and ZnO–AL/XG were 31.89 nm and 28.20 nm, respectively, as summarized in Table 1.

Table 1 gives the typical values of crystallite size of ZnO-XG/AL as calculated using Scherrer`s equation. The average crystallite size of ZnO-XG/AL is smaller than the average crystallite size of ZnO-AL. The average crystallite size of the photocatalyst ZnO synthesized using aloe vera indicates that the xanthan gum as a modifier can inhibit the growth of crystal particles in ZnO-AL/XG and improve particle size uniformity. It was confirmed in previous research [25].

3.1.3 Diffuse Reflectance Ultraviolet (DR-UV) spectroscopy

Diffuse reflectance ultraviolet (DR-UV) spectroscopy was used to examine the optical properties, electronic band structure, and energy band gap of ZnO–AL and ZnO–AL/XG. As illustrated in Figure 5, the absorption spectra of both samples showed absorption edges in the 200–800 nm range, characteristic of semiconductor materials. Figure 5 demonstrates that the addition of the xanthan gum modifier allows the ZnO absorption band shifted to shorter wavelengths (blue shift), indicating a decrease in

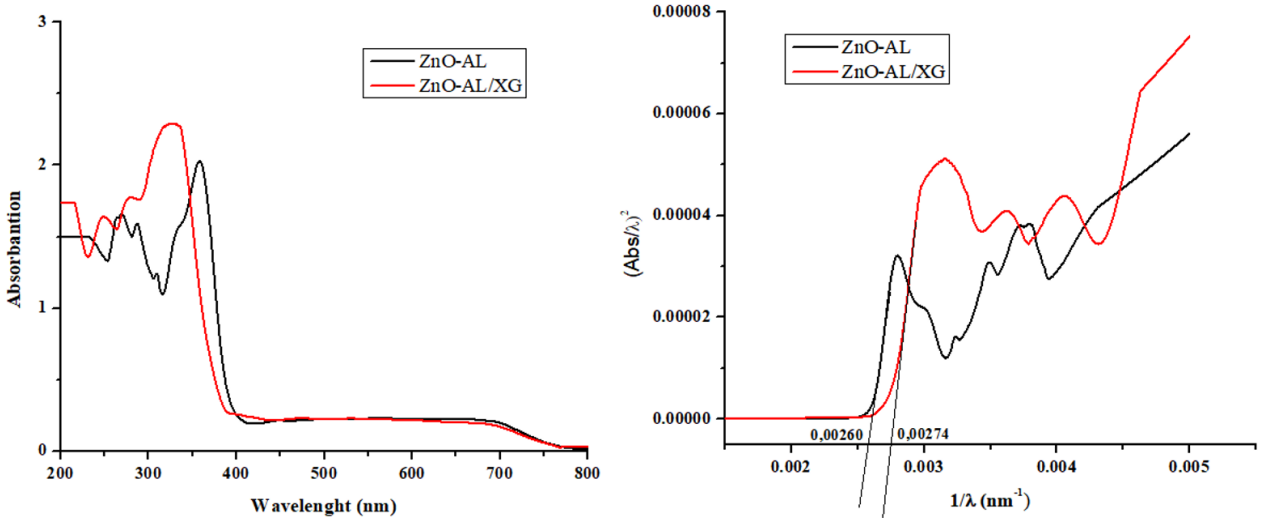

Figure 5. Ultraviolet spectra of ZnO-AL/XG and ZnO-AL.

Table 1. The average crystallite size of ZnO-AL (a) and the average crystallite size of ZnO-AL/XG (b).

dhkl	2θ (deg)	2θ (rad)	FWHM β (deg)	FWHM β (rad)	Particle size D (nm)
100	31.8060	0.5551	0.3110	0.00542	26.56
002	34.4370	0.6010	0.1830	0.00319	45.44
101	36.2930	0.6334	0.3290	0.00574	25.41
102	47.5800	0.8304	0.2500	0.00436	34.72
110	56.6200	0.9882	0.3300	0.00575	27.34
(a) Particle size average					31.89 nm

dhkl	2θ (deg)	2θ (rad)	FWHM β (deg)	FWHM β (rad)	Particle size D (nm)
100	31.7730	0.5545	0.3540	0.00617	23.33
002	34.4260	0.6008	0.2300	0.00401	36.15
101	36.2400	0.6325	0.3400	0.00593	24.58
102	47.4800	0.8286	0.3900	0.00680	22.25
110	56.5740	0.9874	0.2600	0.00453	34.69
(b) Particle size average					28.20 nm

ZnO particle size [25]. These findings are consistent with particle-size determination results, which show that ZnO-AL/XG particles are smaller than ZnO-AL particles. The particle size values were validated using the Scherrer equation, as previously discussed. Table 2 shows the band gap energies of ZnO-Al and ZnO-Al/XG, which were calculated using the Absorption Spectrum Fitting (ASF) technique. The band gap (E_g) in electron volts was determined by extrapolating the linear part of the absorbance of ZnO-Al and ZnO-Al/XG, and the edge wavelength was derived by extending the wavelength curve (Figure 5) until it crossed the X-axis, as follows:

$$E_g = 1239.83/\lambda \quad (8)$$

As can be seen in Table 2, the estimated E_g value for ZnO-AL/X was 3,39 eV, while ZnO-AL presented a lowes E_g values i.e. 3.19 eV. These values are closer to the commonly reported E_g for ZnO [26]. Differences in E_g values can also be caused by differences in the organic compounds present in each compound. This indicates that the xanthan gum modifier in the solution matrix for ZnO-AL/XG disperses the particles and improves particle size uniformity. Differences in E_g values can also be induced by the existence of various polysaccharide molecules within each substance. It implies that the xanthan gum modifier in the ZnO-AL/XG solution matrix disperses particles and enhances particle size uniformity [27]. The results of determining optical properties using DRS showed that the ZnO-AL photocatalyst without xanthan gum resulted in an increase in particle size that grew sporadically and unevenly, thus impacting a smaller band gap energy. Therefore, in the ZnO photocatalysts with increasing particle size, the band gap energy decreases [28].

3.1.4 SEM images

In this study, a scanning electron microscope (SEM) was used to analyze the morphology of the ZnO nanoparticle. The morphology of the ZnO for ZnO-AL/XG and ZnO-AL/XG can be observed from SEM images in Figure 6. Figure 6 illustrates that ZnO nanoparticle in ZnO-AL/XG was homogenously distributed with near-hexagonal shape ((a) and (b)), while in the other image represents the shape and surface texture changes

Table 2. The band gap energy of ZnO-AL and ZnO-AL/XG.

Type ZnO Nanoparticle	Wavelength Edge, λ_g (nm)	E_g (eV)
ZnO-AL	384.61	3.19
ZnO-AL/XG	364.96	3.39

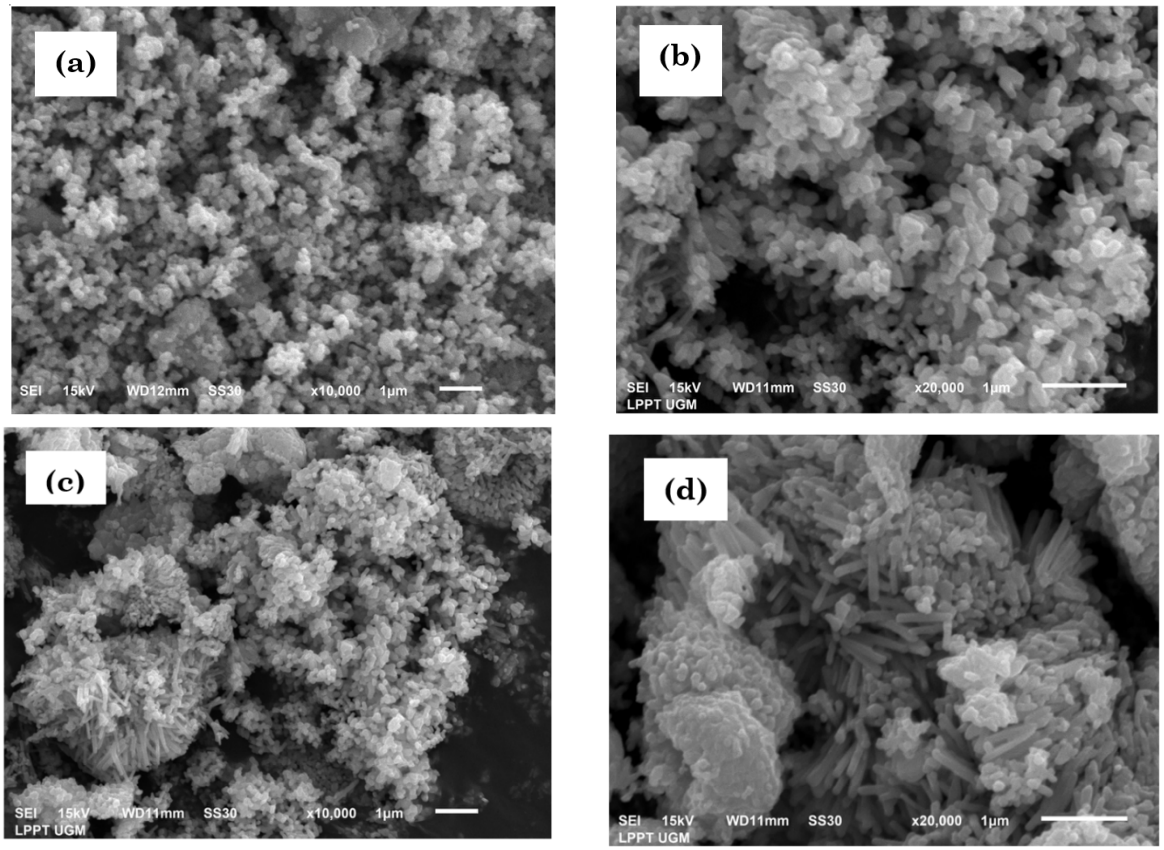

Figure 6. SEM images of (a) and (b) ZnO-AL/XG and SEM image of (c) and (d) ZnO-AL.

of ZnO nanoparticles, which tend to agglomerate and aggregate metal ions on the ZnO nanoparticles in ZnO-AL ((c) and (d)). One difficulty with using reducing agents from plant extracts is that they tend to agglomerate. The use of biopolymers can inhibit erratic crystal growth by forming polysaccharide chains within the matrix, preventing ZnO nanoparticles from aggregating and metal ion aggregation [29]. The synthesis process that occurs during the condensation step provides a homogenous dispersion of spherical particles, as previously reported, the plant-based synthesis of ZnO NPs using aloe vera leaf extract forms ZnO nanoparticles with a spherical lattice shape [30]. The image shows an increase in surface roughness throughout the entire surface of ZnO nanoparticles following using xanthan gum as a modifier. It is also possible to see the macroreticular structure of ZnO particles on the surface of ZnO-AL/XG. The image's homogenous dispersion and fuzzy surface show that the polymer layer on the surface of ZnO particles interacts with the xanthan gum matrix, as previously reported [31].

3.1.5 Transmission Electron Microscopy (TEM)

The structure profiles of ZnO-AL and Zn-AL/XG obtained from green synthesis, as well as some properties such as crystal size, shape, and orientation, have been investigated using TEM, as shown in Figure 7. The TEM image of Zn-AL/XG (A) shows hexagonal, monodispersed ZnO crystal particles that are more evenly and widely distributed on the photocatalyst surface compared to those in ZnO-AL, which appear clumped, stacked and some of the particles are not entirely separated (B). Based on the TEM images, it is confirmed that the xanthan gum modifier helps disperse the ZnO photocatalyst nanoparticles, consistent with the SEM results. Figure 7 shows that ZnO-AL/XG and ZnO-AL have a hexagonal wurtzite crystal structure that is found to dominate the (1 0 0) and (1 0 1) planes oriented towards ZnO NPs. The TEM image of ZnO-Al/XG appears uniform, well-dispersed, and less agglomerated than that of ZnO-AL. Xanthan gum, as a modification, prevents agglomeration due to its reliable chemical structure, thereby enhancing dispersion. The TEM results displayed that the ZnO nanoparticles are more homogeneously dispersed in ZnO-AL/XG.

3.2 The Effect of Contact Time and pH on the Photocatalytic Degradation of Anionic and Cationic Dyes by ZnO-AL and ZnO-AL/XG in Aqueous Solution

The study on the photodegradation properties was conducted by preparing two types of ZnO photocatalysts (Zn-AL and Zn-AL/XG) with different dye concentrations: 25 and 50 mg/L for RY and 10 and 20 mg/mL for RB. The parameters affecting the photocatalytic oxidation process of these ZnO photocatalysts were investigated under varying contact time and pH conditions. The photocatalyst was then irradiated with UV light for 0, 60, 120, 180, 240, 300, and 360 minutes, and the solution was sequentially adjusted to pH 2, 4, 6, 8, 10, and 12 to evaluate the effects of contact time and pH.

The effect of these parameters on the photocatalytic degradation of RY and RB by ZnO photocatalysts was evaluated using spectrometric analysis. Upon irradiation ($\lambda \leq 380$ nm), photons are absorbed by the ZnO semiconductor, leading to the excitation of electrons and the generation of

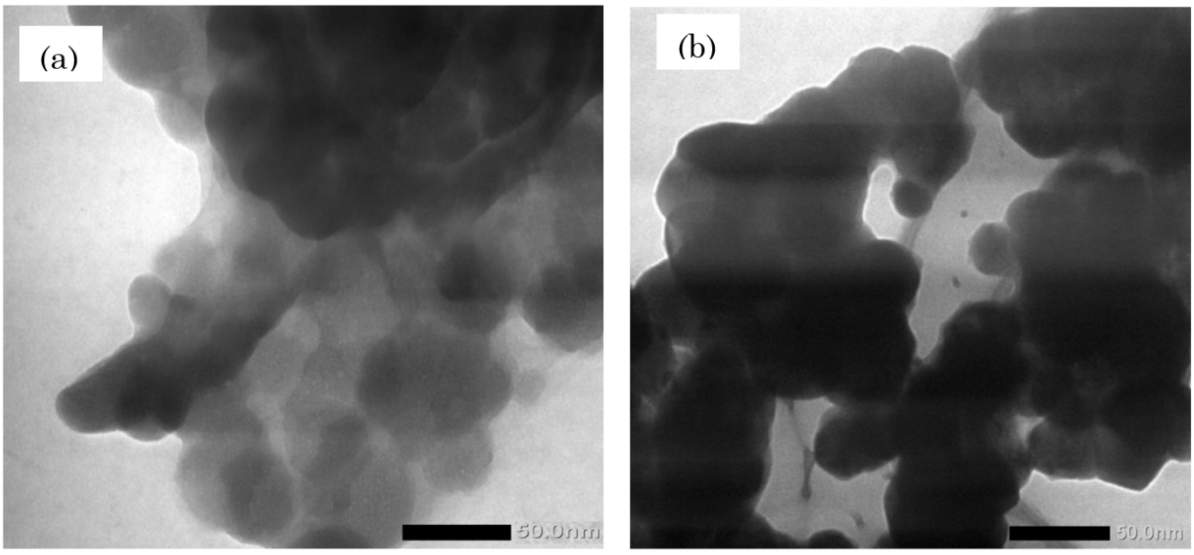

Figure 7. TEM images of (a) ZnO-AL/XG and (b) ZnO-AL at magnification scale of 50 nm.

electron–hole (e^-/h^+) pairs, with holes (h^+) in the valence band (VB) and electrons (e^-) in the conduction band (CB). The photocatalytic process can be represented by the following reactions [32]:

$$ZnO + h\nu\ (\lambda \leq 380\ nm) \rightarrow ZnO\ (e^-_{CB} + h^+_{VB}) \quad (8)$$
$$ZnO\ (e^-_{CB} + h^+_{VB}) \rightarrow Energy \quad (9)$$

In Equations (8) and (9), the electrons excited from the valence band (VB) to the conduction band (CB) react with dissolved oxygen molecules to generate superoxide radicals ($O_2^{\bullet -}$), which subsequently form hydroxyl radicals (•OH).

$$O_2 + e^-_{CB} \rightarrow O_2^{\bullet -} \quad (10)$$
$$H_2O + h^+_{VB} \rightarrow \cdot OH + H^+ \cdot \quad (11)$$

This superoxide radical species helps decompose dyes in aqueous solutions, simultaneously inducing secondary degradation, as presented in Figures 8. The presence of positive holes (h^+) in the valence band drives oxidation during this reaction. No hydrogen ions (H^+) or hydroxyl radicals(•OH) are produced during this process (Equations 10 and 11). Residual organic pollutants are degraded through radical action to produce H_2O and CO_2 [33].

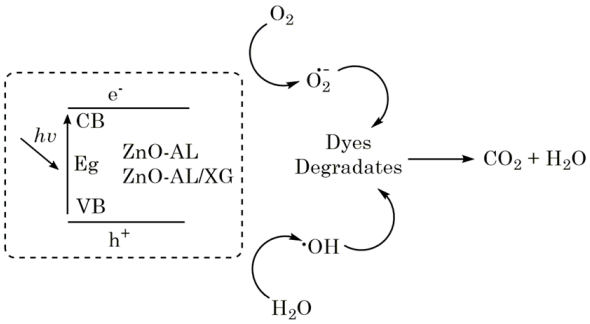

Figure 8. Photodegradation mechanism of dyes by ZnO-AL and ZnO-AL/XG photocatalysts.

$$O_2^{\bullet -} + h^+_{VB} \rightarrow \bullet OH \quad (12)$$
$$\bullet OH_2 + \bullet OH_2 \rightarrow H_2O_2 + O_2 \quad (13)$$
$$O_2^{\bullet -} + \bullet OH_2 \rightarrow O_2. + HO_2^- \quad (14)$$
$$HO_2^- + h^+_{VB} \rightarrow H_2O_2 \quad (15)$$
$$H_2O_2 + h\nu \rightarrow 2 \bullet OH \quad (16)$$
$$O_2^{\bullet -} + H_2O_2 \rightarrow \bullet OH + OH^- + O_2 \quad (17)$$
$$H_2O_2 + e^-_{CB} \rightarrow OH^- \bullet OH \quad (18)$$
$$\bullet OH + dyes \rightarrow O_2 + CO_2. + H_2O \quad (19)$$
$$O_2^{\bullet -} + dyes \rightarrow CO_2 + H_2O \quad (20)$$

These superoxide radical species play a crucial role in the degradation of environmental pollutants, not only as primary oxidizing agents but also by facilitating secondary degradation pathways. Concurrently, oxidation reactions occur at the valence band h^+_{VB} due to the presence of positive holes (h^+). In this process, no hydrogen ions (H^+) or hydroxyl radicals (•OH) are directly generated, as illustrated in Figure 8. Persistent organic pollutants are degraded by these radicals and pollutants convert into H_2O and CO_2.

Figures 9 – 10 demonstrates that the photocatalytic degradation efficiency of ZnO–AL is lower than that of ZnO–AL/XG. This difference may be attributed to the smaller ZnO–AL/XG crystallite size, which induces quantum-size effects an increases the band-gap energy, thereby enhancing photocatalytic activity. Furthermore, the reduced particle size provides a higher specific surface area, thereby facilitating more effective contact between the photocatalyst and the dye molecules. As a result, ZnO–AL/XG exhibits superior degradation performance.

These results are consistent with the previous discussion (Figures 4 and 5), showing that ZnO

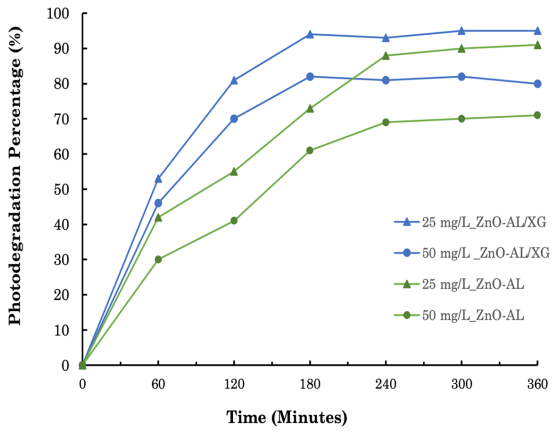

Figure 9. The effect of contact time on the photocatalytic degradation of Remazol Yellow (RY) at 25 mg/L and 50 mg/L, by Zn-O/AL and ZnO-AL/XG, each with a dosage of 1 gram.

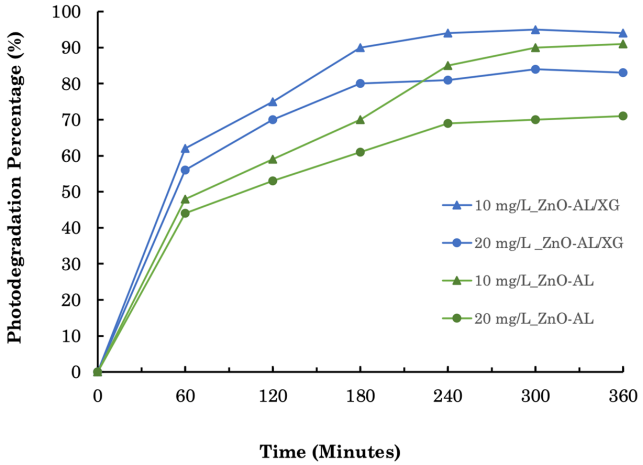

Figure 10. The effect of contact time on the photocatalytic degradation of Rhodamine B (RB) at 10 mg/L and 20 mg/L, by Zn-O/AL and ZnO-AL/XG, each with a dosage of 1 gram.

synthesis modified with xanthan gum results in a decrease in particle size, thereby increasing the band gap energy, which consequently reduces the electron-hole pair recombination rate in the photocatalyst. The physical properties of the carbohydrates in xanthan gum can also form a hydrogel, helping to structure the zinc oxide and producing porous nanoparticles. It enhances the photocatalytic efficiency of the resulting zinc oxide by increasing surface adsorption and the number of accessible reaction sites, thereby providing more light-generated electrons and holes. It is valuable for the application of dye wastewater treatment in aquatic environments. The study also revealed that the optimum photocatalytic activity was achieved at a contact time of 240 minutes for both RY and RB dyes. Beyond this duration, no significant enhancement in degradation efficiency was observed, indicating that the process had reached equilibrium.

The initial dye concentration also influences the percentage of photodegradation. The effect of the initial dye concentration on the photocatalytic degradation of ZnO-AL and ZnO-AL/XG was evaluated using 25 and 50 mg/L for RY and 10 and 20 mg/L for RB. A lower concentration of RB is required because its absorptivity coefficient is high, resulting in a highly colored solution. In general, it can be observed that the percentage of photodegradation for all variations of dye concentration significantly decreases with the increase in initial dye concentration. This decrease is related to the reduced capacity of the ZnO-AL and ZnO-AL/XG photocatalysts to adsorb ion groups from dye compounds on the photocatalyst surface as the concentrations of RY and RB increase. In previous research, it was mentioned that the process of ZnO nanoparticle adsorption onto dye molecules before photocatalysis is an important factor in degradation. Therefore, a higher amount of adsorbed dye is usually followed by an increase in degradation process [34].

In several previous studies, the degradation mechanism of RB is as shown in Figure 11. The first step involves N-de-ethylation because the highly reactive hydroxyl radicals attack the N-ethyl at the N-site to break it. This result is confirmed by the LC-ESIMS/MS method. The decolorization of RhB is primarily caused by the cleavage of the conjugated chromophoric group structure, which results from hydroxyl radicals attacking the central carbon atom of RhB. Thus, the N-de-ethylated intermediates are also attacked by hydroxyl radicals, forming several primary oxidation products, such as benzyloxyamine, organic acids like benzoic acid and phthalic acid, which eventually form simple minerals such as CO_2 and H_2O [35].

Meanwhile, the degradation mechanism of RY is shown in Figure 12. Analysis of the RY structure shows that the phi bonds and double bonds in the aromatic rings influence the color intensity. The cleavage of the main chain of the RY compound structure is initiated by the oxidation of the azo group (–N=N–) by hydroxyl radicals, thus initiating the degradation of the more complex compound. The presence of π-bonds in the aromatic rings tends to be unstable, making them easily attacked by hydroxyl radicals (•OH), which then undergo oxidation to form simpler species [36].

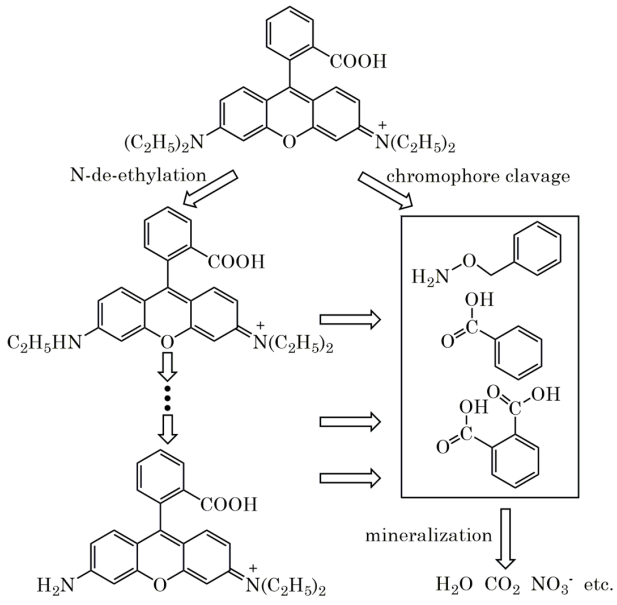

Figure 11. The reaction mechanism for the photodegradation of RB.

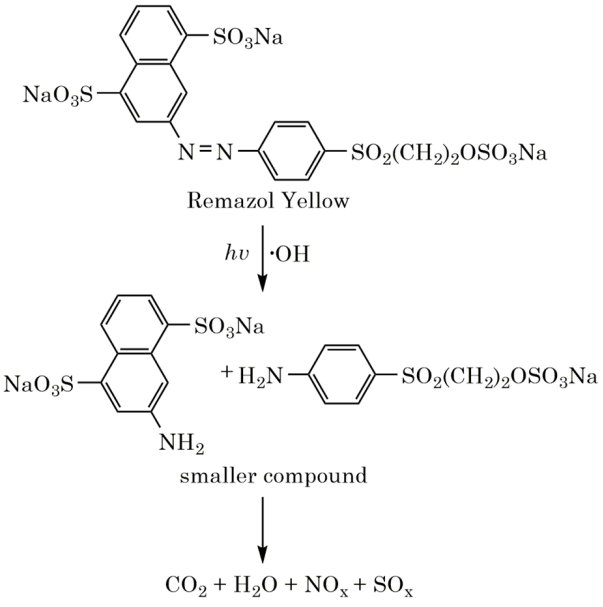

Figure 12. Reaction mechanism of RY photodegradation.

The initial pH of the medium solution is another property that influences the photocatalytic degradation of the dye. The pH of medium solution affects the ionization properties of the dye compound, as well as the electric charge and ionization on the catalyst surface [37]. The effect of pH on the photocatalytic degradation of RY and RB is shown in Figure 13 and Figure 14. The results indicate that the optimum photocatalytic degradation of RY and RB using ZnO–AL and ZnO–AL/XG photocatalysts was achieved at pH of 8 for RY and pH of 10 for RB. The effect of pH on the photocatalytic process can be attributed to the ionization state of the dye molecules as well as the surface charge characteristics of the photocatalyst. Electrostatic interactions play a key role in this mechanism: when the dye molecules and the ZnO surface carry opposite charges, attractive interactions occur, enhancing the adsorption of the dye onto the photocatalyst surface and subsequently accelerating degradation. Conversely, when both possess similar charges, electrostatic repulsion reduces adsorption efficiency, thereby inhibiting the degradation process [38].

The electrostatic properties of the ZnO surface in solution are affected by the pH of the solution, notably between pH of 7.2 and pH of 12, because of the change of colloidal $Zn(OH)_{2(s)}$ solid into $Zn(OH)_{2(aq)}$ ions. A previous study on the surface potential of zinc oxide found that the point of zero charge and charge reversal are directly proportional to zinc ion concentration [37]. The pH-induced change in the surface charge properties of ZnO nanoparticles affects the production of free radicals and the photocatalytic degradation process. Increasing the pH level throughout the procedure might cause fluctuations in the production of •OH radicals, which are important for oxidizing organic compounds such as dyes in aqueous solution. Figures 13 and 14 show that pH influences the photodegradation process of RY and RB. This effect is induced by the function of pH in changing the surface charge of the photocatalyst ZnO as well as the ionization state of the dye molecules due to in the acid-base equilibrium reaction. As be expressed as follows [38]:

$$Zn-OH + H^+ \leftrightarrows Zn-OH_2^+ \quad (21)$$

$$Zn-OH + OH^- \leftrightarrows Zn-O^- + H_2O \quad (22)$$

The ZnO surface exhibits a neutral charge at its point of zero charge (pH_{pzc}), which occurs at pH 9. At this pH, the predominant species is $Zn(OH)_2$. When the pH is below the pH_{pzc}, ZnO tends to form positively charged species, such as Zn^+ and $Zn(OH)^+$. Conversely, at pH values above the pH_{pzc}, negatively charged species, including $Zn(OH)_3^-$ and $Zn(OH)_4^{2-}$, become dominant. The distribution of ZnO species as a function of pH is illustrated in Figure 15 [39,40].

During the dye degradation process, pH affects the surface charge of both the ZnO

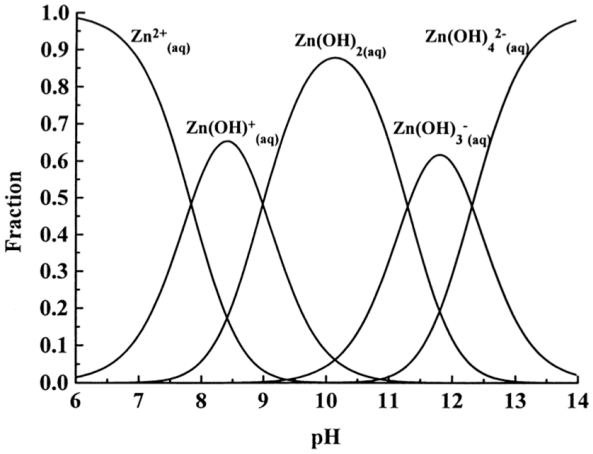

Figure 15. The effect of pH on the speciation fraction of ZnO in solution.

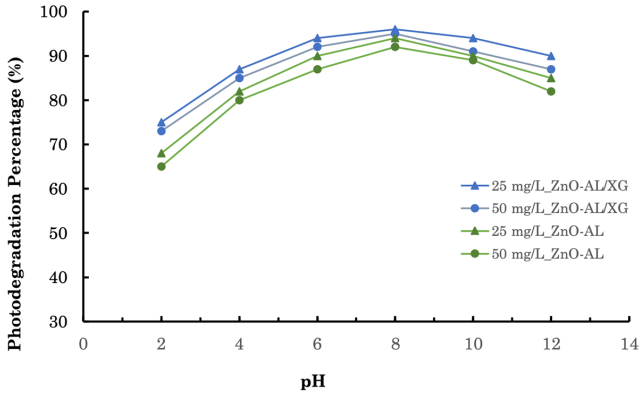

Figure 13. The effect of pH on the photocatalytic degradation of Remazol Yellow (RY) at 25 mg/L and 50 mg/L, by Zn-O/AL and ZnO-AL/XG, each with a dosage of 1 gram.

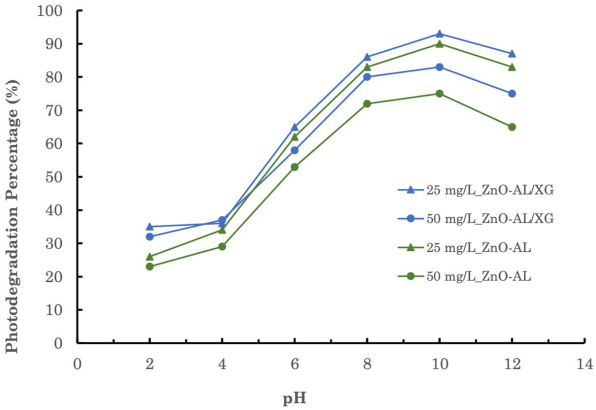

Figure 14. The effect of pH on the photocatalytic degradation of Rhodamine B (RB) at 10 mg/L and 10 mg/L, by Zn-O/AL and ZnO-AL/XG, each with a dosage of 1 gram.

photocatalyst and the dye molecules, thereby determining their interaction and adsorption on the catalyst surface. The cleavage of water molecules induced by the ZnO photocatalyst under UV light irradiation will generate OH radical species on the catalyst surface, as shown in Equations 23 and 24 [41]:

$$OH + h^+ \rightarrow \cdot OH \quad (23)$$

$$H_2O + h^+ \rightarrow \cdot OH + H^+ \quad (24)$$

The hydroxyl radicals act as strong oxidizing agents. Hydroxyl radicals break the azo bonds (-NN-) in azo dyes and reactive dyes, leading to the degradation of RY. In alkaline solutions, photocatalytic degradation is enhanced because the production of ·OH is favoured. However, in acidic solutions, H^+ ions interact with the azo bonds in the dye, making them electron-deficient and more susceptible to ·OH attack [42]. At higher alkaline media, the photocatalytic degradation of RY decreases due to hydroxylation on the catalyst surface, which creates a negative charge that repels RY molecules.

As shown in Figure 15, the distribution diagram for zinc species as a function of solution pH affects the electrostatic properties of the photocatalyst. The surface charge of ZnO affects the interactions and adsorption of both dye molecules due to changes in electrostatic attraction between the molecules. RY is an anionic dye, and RB is a cationic dye, whose ionization properties are affected by pH. The ionization equilibrium of RY and RB are shown on Figures 16 and 17. As shown in Figure 16, the photocatalytic degradation of Rhodamine B (RB) is influenced by pH. The degradation of RB increases slowly from pH of 2 to pH of 4, sharply from pH of 6 to pH of 8, and then gradually decreases from pH of 10 to pH of 12. The degradation process changes throughout the pH range due to the cationic properties of the dye and the presence of carboxyl groups, as illustrated in Figure 17. This behaviour is primarily due to the cationic properties of RB, which contain carboxyl groups in its molecular structure, resulting in electrostatic interactions between RB molecules and the photocatalyst surface. It also illustrates that RB is amphoteric, although it predominantly exists as a cation in solution [43].

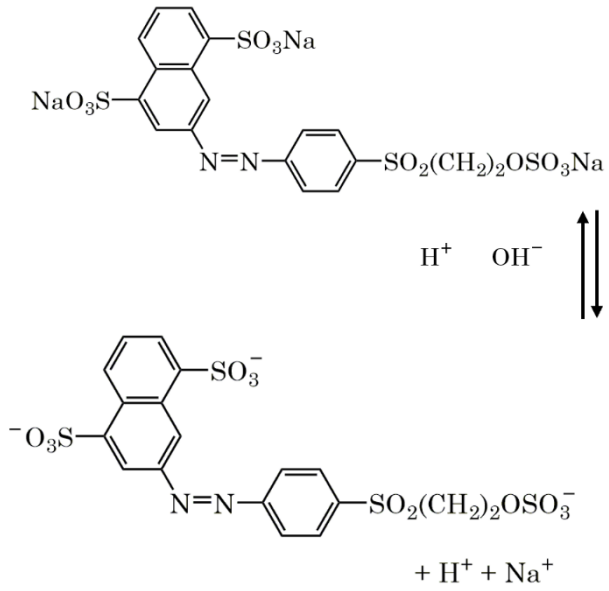

Figure 16. The effect of pH on the ionization of Remazol Yellow.

The photodegradation processes of anionic and cationic dyes using ZnO-AL and ZnO-AL/XG are generally preferred under alkaline conditions. In alkaline solutions, the ZnO surface becomes negatively charged due to adsorbed hydroxide ions, facilitating the formation of hydroxyl radicals (·OH). The increased availability of adsorbed hydroxide ions enhances the formation of these reactive species, thus accelerating the degradation of organic dyes.

3.3 Recycling/Reuse of the ZnO-AL and ZnO-AL/XG Photocatalyst

It is important to determine the stability and durability of photocatalysts to enhance their performance in treating actual wastewater. The reusability of the same photocatalyst was evaluated in three experiments in this work. The results are shown in Figures 18 and 19. For each go-on experiment, the same photocatalyst was used to degrade fresh RY and RB solutions under the same conditions. To evaluate its reusability, the photocatalyst was filtered, washed, and dried before being utilized in the prior experiment.

As seen in Figures 18 – 19, the percentage of RY and RB photodegradation decreased slightly

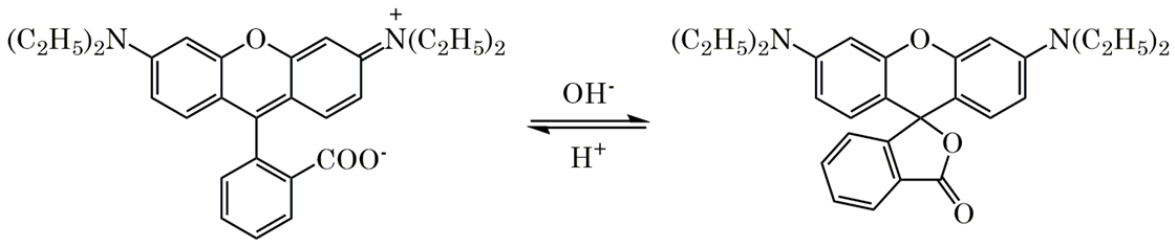

Figure 17. The effect of pH on the ionization of Rhodamine B.

after the second round/cycle. The results show that the photocatalytic activity of ZnO-Al and ZnO-AL/XG also gradually decreased in the third application and continued to decline to approximately 64.46% and 45.76% for RY by ZnO-AL/XG and ZnO-AL, respectively. Similar results were also obtained for RB, with 62.38% and 43.85% for ZnO-AL/XG and ZnO-AL, respectively. The decrease in the percentage of photodegradation may be due to the blocking of the photocatalyst's surface-active sites by intermediate products or by RY and RB molecules remaining in the nanocomposite material, which could not be completely desorbed during photocatalyst washing. The effectiveness and reusability of nanoparticles can be affected by previous dye adsorption, while initially it can enhance dye removal. Additionally, the desorption of dye molecules from the ZnO surface during UV exposure can impact on the effectiveness of dye degradation [44].

However, the percentage photodegradation results of 64.46 % for RY and 62.38 % for RB up to the third use of the photocatalyst indicate that the ZnO-AL/XG photocatalyst can be reused with an ability to remove dyes > 50%. The evaluation results of this photocatalyst reuse show that ZnO nanoparticles synthesized using aloe vera and xanthan gum can function as an effective and efficient photocatalyst in removing dyes from solution.

4. Conclusions

ZnO nanoparticle photocatalysts have been successfully formed through a green synthesis route using aloe vera extract (ZnO-AL) and xanthan gum as modifiers (ZnO-AL/XG). Aloe vera extract functions as a reducing and stabilizing agent, while xanthan gum—a biopolymer in the polysaccharide group—can prevent ZnO nanoparticles from agglomerating and prevent metal ion aggregation, leading to smaller, more uniform particles. The photocatalyst synthesized using aloe vera extract without xanthan gum still tends to form agglomerations, thus requiring the right concentration and composition of xanthan gum for the success of this green synthesis. The characterization results show that the photocatalyst ZnO-AL/XG has a smaller particle size and a larger band gap energy than the photocatalyst ZnO-AL. The results of the photocatalytic degradation study of the anionic dye RY and the cationic dye RB indicate that the smaller ZnO nanoparticle size shows higher photocatalytic activity. Experimental parameters, including contact time and pH, significantly affect photocatalytic activity. Optimum photocatalytic degradation is achieved at a contact time of 240 minutes for RY and RB, and at pH of 8 and pH of 10 for RY and RB, respectively. Under these experimental conditions, the photodegradation percentage of RY and RB by ZnO-AL/XG is higher than that by ZnO-AL, using dosage of 1 g of each ZnO photocatalyst under UV irradiation. From the recycling study of ZnO-AL/Xg and ZnO-AL, it was observed that the photocatalyst still removed the color from the RY and RB solutions up to 3 uses, with photodegradation percentages above 50%. These findings should indicate that the ZnO photocatalyst formed through green synthesis can be used at relatively low cost, while also being highly beneficial in practical applications such as dye wastewater treatment.

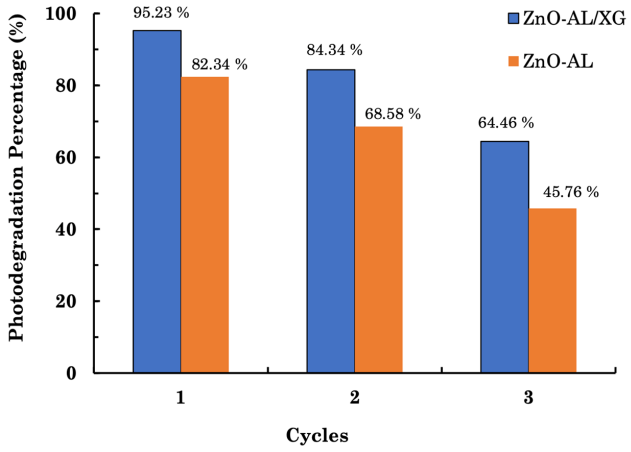

Figure 18. Recycle and reuse of ZnO-AL and ZnO-AL/XG photocatalyst for RY photocatalytic degradation (RY concentration: 25 mg/L; ZnO-AL and ZnO-AL/XG dosage 1 g, pH 8; irradiation time: 240 minutes).

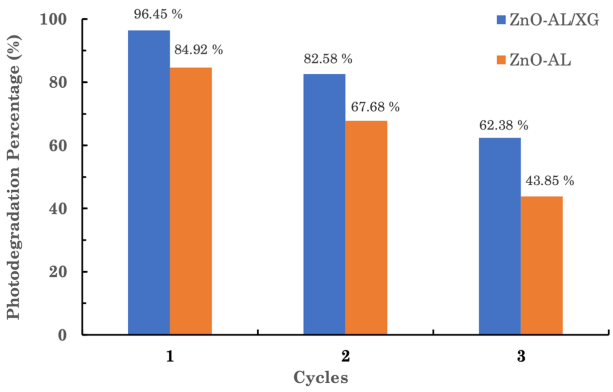

Figure 19. Recycle and reuse of ZnO-AL and ZnO-AL/XG photocatalyst for RB photocatalytic degradation (RB concentration: 10 mg/L; ZnO-AL and ZnO-AL/XG dosage 1 g, pH 10; irradiation time: 240 minutes).

Acknowledgment

This research was financially supported by a grant (2023-2024) to the first author (IF) from the Institute for Research and Community Service, UIN Sunan Kalijaga.

CRedit Author Statement

Author Contributions: I. Fajriati: Conceptualization, Methodology, Validation, Formal analysis, Investigation, Resources, Writing - Original Draft, Supervision, Project administration; P.D. Widiakongko: Software, Validation, Formal analysis, Writing - Review & Editing, Visualization; D. Krisdiyanto: Software, Validation, Writing - Review & Editing, Supervision; H. Hermawati: Formal analysis, Investigation, Resources, Data Curation. All authors have read and agreed to the published version of the manuscript.

References

[1] Hassani, A., Pourshirband, N., Sayyar, Z., Eghbali, P. (2025). Fenton and Fenton-like-based advanced oxidation processes. In: *Innovative and Hybrid Advanced Oxidation Processes for Water Treatment*. 1st Edition - November 5, 2024, 171–203. DOI: 10.1016/B978-0-443-14100-3.00006-5.

[2] Lama, G., Meijide, J., Sanromán, A., Pazos, M. (2022). Heterogeneous Advanced Oxidation Processes: Current Approaches for Wastewater Treatment. *Catalysts*, 12(3), 344. DOI: 10.3390/catal12030344.

[3] Swain, M., Mishra, D. & Sahoo, G. A (2025) review on green synthesis of ZnO nanoparticles. *Discov. Appl. Sci.* 7, 997. DOI: 10.1007/s42452-025-06957-8

[4] Nandhin, J., Karthikeyan, E., Rajeshkumar, S. (2024). Green synthesis of zinc oxide nanoparticles: Eco-friendly advancements for biomedical marvels. *Resources Chemicals and Materials*, 3(4), 294–316. DOI: 10.1016/j.recm.2024.05.001.

[5] Al-darwesh, M.Y., Ibrahim, S.S., Mohammed, M.A. (2024). A review on plant extract mediated green synthesis of zinc oxide nanoparticles and their biomedical applications. *Results in Chemistry*, 7, 101368. DOI: 10.1016/j.rechem.2024.101368.

[6] Dey, S., Mohanty, D. lochan, Divya, N., Bakshi, V., Mohanty, A., Rath, D., Das, S., Mondal, A., Roy, S., Sabui, R. (2025). A critical review on zinc oxide nanoparticles: Synthesis, properties and biomedical applications. *Intelligent Pharmacy*, 3(1), 53–70. DOI: 10.1016/j.ipha.2024.08.004.

[7] Karam, S.T.; Abdulrahman, A.F. (2022) Green Synthesis and Characterization of ZnO Nanoparticles by Using Thyme Plant Leaf Extract. *Photonics*, 9, 594. DOI: 10.3390/photonics9080594.

[8] Ong, C.B., Ng, L.Y., Mohammad, A.W. (2018). A review of ZnO nanoparticles as solar photocatalysts: Synthesis, mechanisms and applications. *Renewable and Sustainable Energy Reviews*, 81, 536–551. DOI: 10.1016/j.rser.2017.08.020.

[9] Suresh, R., Rajendran, S., Hoang, T.K.A., Vo, D.-V.N., Siddiqui, M.N., Cornejo-Ponce, L. (2021). Recent progress in green and biopolymer based photocatalysts for the abatement of aquatic pollutants. *Environmental Research*, 199, 111324. DOI: 10.1016/j.envres.2021.111324.

[10] Hussain, A., Ali, S., Rizwan, M., Zia ur Rehman, M., Javed, M.R., Imran, M., Chatha, S.A.S., Nazir, R. (2018). Zinc oxide nanoparticles alter the wheat physiological response and reduce the cadmium uptake by plants. *Environmental Pollution*, 242, 1518–1526. DOI: 10.1016/j.envpol.2018.08.036.

[11] Sangeetha, G., Rajeshwari, S., Venckatesh, R. (2011). Green synthesis of zinc oxide nanoparticles by aloe barbadensis miller leaf extract: Structure and optical properties. *Materials Research Bulletin*, 46 (12), 2560–2566. DOI: 10.1016/j.materresbull.2011.07.046.

[12] Singh, S.P., Singh, D. (2010). Biodiesel production through the use of different sources and characterization of oils and their esters as the substitute of diesel: A review. *Renewable and Sustainable Energy Reviews,* 14, 200–216. DOI: 10.1016/j.rser.2009.07.017.

[13] Rasli, N.I., Basri, H., Harun, Z. (2020). Zinc oxide from aloe vera extract: two-level factorial screening of biosynthesis parameters. *Heliyon*, 6(1), e03156. DOI: 10.1016/j.heliyon.2020.e03156.

[14] Pauzi, N., Zain, N.M., Yusof, N.A.A. (2020). Gum arabic as natural stabilizing agent in green synthesis of ZnO nanofluids for antibacterial application. *Journal of Environmental Chemical Engineering*, 8(3), 103331. DOI: 10.1016/j.jece.2019.103331.

[15] Wu, C., Zhang, T., Ji, B., Chou, Y., Du, X. (2024). Green Synthesis of Zinc Oxide Nanoparticles Using Aloe vera Leaf Extract and Evaluation of the Antimicrobial and Antioxidant Properties of the ZnO/Regenerated Cellulose Film. *Cellulose*, 31(8), 4849–4864. DOI: 10.1007/s10570-024-05914-9.

[16] Khaldoune, K., Rafya, M., Louchachha, I., Hasnaoui, A., Benkhalti, F., Fdil, N., Ait Ali, M. (2025). Study on the biosynthesis and antibacterial effect of Zinc Oxide Nanoparticles using aloe vera latex extract. *Chemical Papers*, 79(8), 5399–5407. DOI: 10.1007/s11696-025-04133-1.

[17] Hnawi, S.K., Nayad, A., Aitdads, H., Agdad, A., Afqir, M., Nkhaili, L., El Firdoussi, L., Oueriagli, A., Ait Ali, M. (2021). Investigation of the Structural, Optical, Electrical, and Dielectrical Properties of Aloe Vera Leaf Exudate. *Journal of Solar Energy Engineering*, 143 (2). DOI: 10.1115/1.4048086.

[18] Alavi, M., Nokhodchi, A. (2021). Synthesis and modification of bio-derived antibacterial Ag and ZnO nanoparticles by plants, fungi, and bacteria. *Drug Discovery Today*, 26(8), 1953–1962. DOI: 10.1016/j.drudis.2021.03.030.

[19] Husain, F.M., Hasan, I., Qais, F.A., Khan, R.A., Alam, P., Alsalme, A. (2020). Fabrication of Zinc Oxide-Xanthan Gum Nanocomposite via Green Route: Attenuation of Quorum Sensing Regulated Virulence Functions and Mitigation of Biofilm in Gram-Negative Bacterial Pathogens. *Coatings*, 10(12), 1190. DOI: 10.3390/coatings10121190.

[20] Abu Elella, M.H., Goda, E.S., Gab-Allah, M.A., Hong, S.E., Pandit, B., Lee, S., Gamal, H., Rehman, A. ur, Yoon, K.R. (2021). Xanthan gum-derived materials for applications in environment and eco-friendly materials: A review. *Journal of Environmental Chemical Engineering*, 9(1), 104702. DOI: 10.1016/j.jece.2020.104702.

[21] Ying, S., Guan, Z., Ofoegbu, P.C., Clubb, P., Rico, C., He, F., Hong, J. (2022). Green synthesis of nanoparticles: Current developments and limitations. *Environmental Technology & Innovation*, 26, 102336. DOI: 10.1016/j.eti.2022.102336.

[22] Wu, C., Zhang, T., Ji, B., Chou, Y., Du, X. (2024). Green Synthesis of Zinc Oxide Nanoparticles Using Aloe vera Leaf Extract and Evaluation of the Antimicrobial and Antioxidant Properties of the ZnO/Regenerated Cellulose Film. *Cellulose*, 31(8), 4849–4864. DOI: 10.1007/s10570-024-05914-9.

[23] Chikkanna, M.M., Neelagund, S.E., Rajashekarappa, K.K. (2019). Green synthesis of Zinc oxide nanoparticles (ZnO NPs) and their biological activity. *SN Applied Sciences*, 1(1), 117. DOI: 10.1007/s42452-018-0095-7.

[24] Almoneef, M., Haia H.A., Hendi, A., Aldehish, Merghani, N.M., Alshammari, S.G. (2024) Exploring the multi-faceted potential: Synthesized ZnO nanostructure – Characterization, photocatalysis, and crucial biomedical applications, *Heliyon*, 10 (12), e32714. DOI: 10.1016/j.heliyon. 2024.e32714.

[25] Nagaraja, K., Mallika, B., Arunpandian, M., Ravindran, E., Hwan, T., (2025) Green synthesis of gold-decorated $BaTiO_3$-ZnO nanocomposites using Arabic gum polymer for efficient photocatalytic degradation of emerging textile dyes, antimicrobial, and toxicological evaluation, *Int. J. Biol. Macromol.* 311, 143396. DOI: 10.1016/j.ijbiomac.2025.143396.

[26] K.S., J., Jose, J., Li, T., Thomas, M., Shankregowda, A.M., Sreekumaran, S., Kalarikkal, N., Thomas, S. (2020). Application of novel zinc oxide reinforced xanthan gum hybrid system for edible coatings. *International Journal of Biological Macromolecules*, 151, 806–813. DOI: 10.1016/j.ijbiomac.2020.02.085.

[27] Abdelbaky, A.S., Mohamed, A.M.H.A., Sharaky, M., Mohamed, N.A., Diab, Y.M. (2023). Green approach for the synthesis of ZnO nanoparticles using Cymbopogon citratus aqueous leaf extract: characterization and evaluation of their biological activities. *Chemical and Biological Technologies in Agriculture*, 10(1), 63. DOI: 10.1186/s40538-023-00432-5.

[28] Dey, S., Mohanty, D. lochan, Divya, N., Bakshi, V., Mohanty, A., Rath, D., Das, S., Mondal, A., Roy, S., Sabui, R. (2025). A critical review on zinc oxide nanoparticles: Synthesis, properties and biomedical applications. *Intelligent Pharmacy*, 3(1), 53–70. DOI: 10.1016/j.ipha.2024.08.004.

[29] Tabassum, Z., Girdhar, M., Kumar, A., Malik, T., Mohan, A. (2023). ZnO Nanoparticles-Reinforced Chitosan–Xanthan Gum Blend Novel Film with Enhanced Properties and Degradability for Application in Food Packaging. *ACS Omega*, 8(34), 31318–31332. DOI: 10.1021/acsomega.3c03763.

[30] Alhujaily, M., Albukhaty, S., Yusuf, M., Mohammed, M.K.A., Sulaiman, G.M., Al-Karagoly, H., Alyamani, A.A., Albaqami, J., AlMalki, F.A. (2022). Recent Advances in Plant-Mediated Zinc Oxide Nanoparticles with Their Significant Biomedical Properties. *Bioengineering*, 9(10), 541. DOI: 10.3390/bioengineering9100541.

[31] El-Kholy, S.A., Radwan, E.K., El-Naggar, M.E., El-Wakeel, S.T., El-Tantawy El Sayed, I. (2023). Sponge-like zinc oxide nanoparticles loaded xanthan gum/cationic chitosan cryogel: Synthesis, characterization, microbicidal and adsorption of synthetic dye and heavy metal. *Journal of Environmental Chemical Engineering*, 11(5), 110652. DOI: 10.1016/j.jece.2023.110652.

[32] Lal, M., Sharma, P., Singh, L., Ram, C. (2023). Photocatalytic degradation of hazardous Rhodamine B dye using sol-gel mediated ultrasonic hydrothermal synthesized of ZnO nanoparticles. *Results in Engineering*, 17, 100890. DOI: 10.1016/j.rineng.2023.100890.

[33] Bhapkar, A.R., Bhame, S. (2024). A review on ZnO and its modifications for photocatalytic degradation of prominent textile effluents: Synthesis, mechanisms, and future directions. *Journal of Environmental Chemical Engineering*, 12(3), 112553. DOI: 10.1016/j.jece.2024.112553.

[34] Amdeha, E., Salem, M. (2022). Facile Green Synthesis of ZnO Supported on Exfoliated Graphite for Photocatalytic Degradation of Dye under UV and Visible-Light Irradiation. *Egyptian Journal of Chemistry*, 0(0), 0–0. DOI: 10.21608/ejchem.2022.130532.5931.

[35] Liang, L., Cheng, L., Zhang, Y., Wang, Q., Wu, Q., Xue, Y., Meng, X. (2020). Efficiency and mechanisms of rhodamine B degradation in Fenton-like systems based on zero-valent iron. *RSC Advances*, 10(48), 28509–28515. DOI: 10.1039/D0RA03125A.

[36] Purnawan, C., Wahyuningsih, S., Aniza, O.N., Sari, O.P. (2021). Photocatalytic Degradation of Remazol Brilliant Blue R and Remazol Yellow FG using TiO2 doped Cd, Co, Mn. *Bulletin of Chemical Reaction Engineering & Catalysis*, 16(4), 804–815. DOI: 10.9767/bcrec.16.4.11423.804-815.

[37] Arab, C., El Kurdi, R., Patra, D. (2022). Effect of pH on the removal of anionic and cationic dyes using zinc curcumin oxide nanoparticles as adsorbent. *Materials Chemistry and Physics*, 277, 125504. DOI: 10.1016/j.matchemphys.2021.125504.

[38] Kazeminezhad, I., Sadollahkhani, A. (2016). Influence of pH on the photocatalytic activity of ZnO nanoparticles. *Journal of Materials Science: Materials in Electronics*, 27(5), 4206–4215. DOI: 10.1007/s10854-016-4284-0.

[39] El-Taib Heakal, F., Abd-Ellatif, W.R., Tantawy, N.S., Taha, A.A. (2018). Impact of pH and temperature on the electrochemical and semiconducting properties of zinc in alkaline buffer media. *RSC Advances*, 8(7), 3816–3827. DOI: 10.1039/C7RA12723E.

[40] Le, A.T., Samsuddin, N.S.B., Chiam, S.-L., Pung, S.-Y. (2021). Synergistic effect of pH solution and photocorrosion of ZnO particles on the photocatalytic degradation of Rhodamine B. *Bulletin of Materials Science*, 44(1), 5. DOI: 10.1007/s12034-020-02281-6.

[41] Siddique, A.B., Shaheen, M.A., Abbas, A., Zaman, Y., Bratty, M.A., Najmi, A., Hanbashi, A., Mustaqeem, M., Alhazmi, H.A., Rehman, Z. ur, Zoghebi, K., Amin, H.M.A. (2024). Thermodynamic and kinetic insights into azo dyes photocatalytic degradation on biogenically synthesized ZnO nanoparticles and their antibacterial potential. *Heliyon*, 10(23), e40679. DOI: 10.1016/j.heliyon.2024.e40679.

[42] Moghaddasfar, A., Darbandi, M., Li, Z.-A. (2023). Mesoporous cobalt oxide nanoparticles synthesized by a sonochemical method in the presence of a deep eutectic solvent for oxidative sonophotocatalytic decomposition of caffeine. *Journal of Water Process Engineering*, 54, 104056. DOI: 10.1016/j.jwpe.2023.104056.

[43] Groeneveld, I., Kanelli, M., Ariese, F., van Bommel, M.R. (2023). Parameters that affect the photodegradation of dyes and pigments in solution and on substrate – An overview. *Dyes and Pigments*, 210, 110999. DOI: 10.1016/j.dyepig.2022.110999.

[44] Rasheed, H.M., Aroosh, K., Meng, D., Ruan, X., Akhter, M., Cui, X. (2025). A review on modified ZnO to address environmental challenges through photocatalysis: Photodegradation of organic pollutants. *Materials Today Energy*, 48, 101774. DOI: 10.1016/j.mtener.2024.101774.